Finite Elements in Analysis and Design 44 (2008) 831 – 841

Contents lists available at ScienceDirect

Finite Elements in Analysis and Design

journal homepage: www.elsevier.com/locate/finel

An efficient adaptive analysis procedure for certified solutions with exact bounds of strain energy for elasticity problems

G.Y. Zhang[a,*], G.R. Liu[a,b], Y. Li[b]

[a]The Singapore-MIT Alliance (SMA), National University of Singapore, E4-04-10, 4 Engineering Drive 3, 117576 Singapore, Singapore
[b]Center for Advanced Computations in Engineering Science (ACES), Department of Mechanical Engineering, National University of Singapore, 9 Engineering Drive 1, 117576 Singapore, Singapore

ARTICLE INFO

Article history:
Received 19 October 2007
Received in revised form 22 May 2008
Accepted 23 June 2008
Available online 12 August 2008

Keywords:
Meshfree methods
Point interpolation method
Strain smoothing
Adaptive analysis
Solution bound
Elasticity problems

ABSTRACT

We present an efficient adaptive analysis procedure to obtain certified solutions of desired accuracy with bounds to the exact solution in energy norm for elasticity problems. The procedure makes the use of the recent finding that the upper bound to the exact strain energy can be obtained using the linearly conforming point interpolation method (LC-PIM), and the well-known fact that the lower bound can be obtained using the standard displacement-based fully compatible finite element method (FEM). To perform the adaptive analysis, a residual error-based error indicator and a simple *h*-type refinement scheme are employed and the relative error of the computed strain energy is used as the global stopping criteria. A number of numerical examples, including problems with singularity, have been studied to demonstrate the effectiveness and efficiency of the present procedure. The numerical results have been found converging very fast to the exact solution, and the bounds to the exact strain energy can be obtained efficiently at any stage in the adaptive process whenever required.

1. Introduction

In the process of designing an advanced engineering system, the underline partial differential equations have to be solved with desired accuracy. Except for some simple models, the differential equations are usually very difficult to solve analytically to obtain exact solutions. Various numerical techniques have been therefore developed to obtain approximate solutions, such as the well-known finite difference method (FDM), widely used finite element method (FEM) and the newly developed meshfree methods [1], etc.

After more than half a century of development, FEM has become one of the most general and powerful tools for numerical simulation in engineering and science [2,3]. It is well known that the fully compatible displacement-based FEM produces an overestimation of the stiffness resulting in an underestimation of strain energy. This property is often used to *estimate* the error of the obtained approximated solution. To certify the approximated solution against to the exact solution that is generally unknown is of very importance and a very challenging task. One way to obtain such a certificate is to use an equilibrium model of FEM [4,5] that is, however, a quite complicated process and may not always doable for general problems.

A linearly conforming point interpolation method (LC-PIM) was developed by combining meshfree techniques with the FEM formulation [6]. In this method, point interpolation method (PIM) is used to construct shape functions with a small set of nodes located in a local support domain. PIM shape functions possessing delta function property are used for straightforward imposition of point essential boundary conditions [7]. Instead of using compatible strains generated from the strain-displacement relation, LC-PIM uses the *smoothed* strains over smoothing cells of the nodes, which can provide *softening* effect to the structure and makes the method possess many good properties [8]. Note that the PIM constructs shape functions using a set of local nodes, in local support domain that can overlap, and hence the order of the shape functions can be as high as desired, as long as the moment matrix is not singular [6]. A more general formulation is the conforming radial PIM (RPIM) [9] that uses randomly distributed local nodes, in which the conformability is achieved using nodal integration with strain smoothing operation. Recently, Liu et al. [10] have also discovered that the strains in a node-based smoothing cell can be piece-wise linearly constructed in a number of ways, and very accurate solution can be obtained. In such a formulation, high order of conformability may be achieved.

It has been found and proven that LC-PIM can provide upper bound solution in energy norm for elasticity problems with homogeneous essential boundary conditions [8]. It implies that using LC-PIM together with the standard displacement-based fully compatible

* Corresponding author. Tel.: +65 65164796.
E-mail address: smazg@nus.edu.sg (G.Y. Zhang).

0168-874X/$ - see front matter © 2008 Elsevier B.V. All rights reserved.
doi:10.1016/j.finel.2008.06.010

FEM, we can now bound the exact strain energy from above and below, respectively. Utilizing these properties, we propose an efficient adaptive analysis procedure to obtain certified solutions of desired accuracy with bounds to the exact strain energy for elasticity problems. In this procedure, the LC-PIM is used to obtain the upper bound, and the standard fully compatible FEM is used to compute the lower bound of the exact solution in energy norm. To perform the adaptive analysis, a residual-based error indicator and a simple *h*-type refinement scheme are employed and the relative error of the computed strain energies is used as the global criteria to determine when to terminate the adaptive process.

The paper is outlined as follows. In Section 2, the displacement-based model of FEM is briefly introduced. In Section 3, the formulae of LC-PIM are presented and some import properties are described. The techniques used in the adaptive analysis, including the residual-based error indicator, the definition of local and global criteria, and a simple *h*-type refinement scheme, are introduced in Section 4. In Section 5, some numerical examples are studied to demonstrate the effectiveness and efficiency of the present procedure for bounding the exact strain energy of elasticity problems. Some concluding remarks are finally made in Section 6.

2. Briefing on the FEM

2.1. Basic equations for linear elasticity

Consider a 2D static elasticity problem which is governed by the following equilibrium equation in the domain Ω bounded by $\Gamma(\Gamma = \Gamma_u + \Gamma_t; \Gamma_u \cap \Gamma_t = 0)$

$$\mathbf{L}_d^{\mathrm{T}}\boldsymbol{\sigma} + \mathbf{b} = 0 \quad \text{in } \Omega \tag{1}$$

where $\boldsymbol{\sigma}$ is the stress tensor in the following vector form:

$$\boldsymbol{\sigma}^{\mathrm{T}} = \{\sigma_{xx} \;\; \sigma_{yy} \;\; \tau_{xy}\} \tag{2}$$

$\mathbf{b}$ is the vector of the body force as follows:

$$\mathbf{b}^{\mathrm{T}} = \{b_x \;\; b_y\} \tag{3}$$

and $\mathbf{L}_d$ is a matrix of differential operator defined as

$$\mathbf{L}_d = \begin{bmatrix} \dfrac{\partial}{\partial x} & 0 \\ 0 & \dfrac{\partial}{\partial y} \\ \dfrac{\partial}{\partial y} & \dfrac{\partial}{\partial x} \end{bmatrix} \tag{4}$$

Essential and natural boundary conditions are given as follows:

$$\begin{aligned} &\mathbf{u} = \hat{\mathbf{u}} \quad \text{on } \Gamma_u \\ &\mathbf{L}_n^{\mathrm{T}}\boldsymbol{\sigma} = \hat{\mathbf{t}} \quad \text{on } \Gamma_t \end{aligned} \tag{5}$$

where $\mathbf{u} = \{u_x \;\; u_y\}^{\mathrm{T}}$ is the vector of displacement, $\hat{\mathbf{u}}$ is the vector of the prescribed displacement on the essential boundary Γ_u, $\hat{\mathbf{t}}$ is the vector of the prescribed traction on the natural boundary Γ_t and $\mathbf{L}_n$ is the matrix of unit outward normal defined as follows:

$$\mathbf{L}_n = \begin{bmatrix} n_x & 0 \\ 0 & n_y \\ n_y & n_x \end{bmatrix} \tag{6}$$

The compatibility equation (strain–displacement relation) is given by

$$\boldsymbol{\varepsilon} = \mathbf{L}_d\mathbf{u} \tag{7}$$

where $\boldsymbol{\varepsilon}$ is the strain tensor in the following vector form

$$\boldsymbol{\varepsilon}^{\mathrm{T}} = \{\varepsilon_{xx} \;\; \varepsilon_{yy} \;\; \gamma_{xy}\} \tag{8}$$

The constitutive equation (stress–strain relation) is given by

$$\boldsymbol{\sigma} = \mathbf{D}\boldsymbol{\varepsilon} \tag{9}$$

where $\mathbf{D}$ is a symmetric positive definite (SPD) matrix of material constants.

2.2. Formulae of FEM

In the FEM, the discrete equations are generated from the standard Galerkin weak form:

$$\int_\Omega (\delta\boldsymbol{\varepsilon})^{\mathrm{T}}\mathbf{D}\boldsymbol{\varepsilon}\,\mathrm{d}\Omega - \int_\Omega (\delta\mathbf{u})^{\mathrm{T}}\mathbf{b}\,\mathrm{d}\Omega - \int_{\Gamma_t} (\delta\mathbf{u})^{\mathrm{T}}\hat{\mathbf{t}}\,\mathrm{d}\Gamma = 0 \tag{10}$$

where $\mathbf{u} \in H^1(\Omega)$ are trial functions with corresponding test function of $\delta\mathbf{u} \in H_0^1(\Omega)$, in which $H^1(\Omega)$ denotes the Sobolev space of functions with square integrable derivatives in $\Omega$and $H_0^1(\Omega)$ is the subset of $H^1(\Omega)$ that satisfy essential boundary conditions in Eq. (5).

The FEM uses the following trial and test functions:

$$\begin{aligned} &\tilde{\mathbf{u}}(\mathbf{x}, \mathbf{d}) = \sum_{i \in n_e} \boldsymbol{\Phi}_i(\mathbf{x})\mathbf{d}_i \\ &\delta\tilde{\mathbf{u}}(\mathbf{x}, \mathbf{d}) = \sum_{i \in n_e} \boldsymbol{\Phi}_i(\mathbf{x})\delta\mathbf{d}_i \end{aligned} \tag{11}$$

where n_e is the number of nodes of the element containing $\mathbf{x}$, $\mathbf{d}_i = [u_{xi} \;\; u_{yi}]^{\mathrm{T}}$ is the nodal displacement vector and

$$\boldsymbol{\Phi}_i(\mathbf{x}) = \begin{bmatrix} \varphi_i(\mathbf{x}) & 0 \\ 0 & \varphi_i(\mathbf{x}) \end{bmatrix} \tag{12}$$

is the matrix of shape functions which satisfy the following conditions:

$$\begin{aligned} &\varphi_i(\mathbf{x}_j) = \delta_{ij} \\ &\sum_{i \in n_e} \varphi_i(\mathbf{x}) = 1 \end{aligned} \tag{13}$$

where δ_{ij} is the Kronecker delta. Substituting Eqs. (11) into Eq. (10) and invoking the arbitrariness of virtual nodal displacements, the standard discretized algebraic system equation can be obtained as

$$\tilde{\mathbf{K}}\tilde{\mathbf{d}} = \tilde{\mathbf{f}} \tag{14}$$

where $\tilde{\mathbf{d}}$ is the vector of nodal displacements containing all the unconstrained nodes, $\tilde{\mathbf{K}}$ is the global stiffness matrix and $\tilde{\mathbf{f}}$ is vector of nodal forces at the unconstrained nodes. The global stiffness matrix and the force vector are assembled using the entries defined as

$$\begin{aligned} &\tilde{\mathbf{K}}_{ij} = \int_\Omega \tilde{\mathbf{B}}_i^{\mathrm{T}}\mathbf{D}\tilde{\mathbf{B}}_j\,\mathrm{d}\Omega \\ &\tilde{\mathbf{f}}_i = \int_\Omega \boldsymbol{\Phi}_i^{\mathrm{T}}(\mathbf{x})\mathbf{b}\,\mathrm{d}\Omega + \int_{\Gamma_t} \boldsymbol{\Phi}_i^{\mathrm{T}}(\mathbf{x})\hat{\mathbf{t}}\,\mathrm{d}\Gamma \end{aligned} \tag{15}$$

where $\mathbf{B}$ is the strain matrix defined as

$$\tilde{\mathbf{B}}_i(\mathbf{x}) = \mathbf{L}_d\boldsymbol{\Phi}_i(\mathbf{x}) = \begin{bmatrix} \dfrac{\partial\varphi_i(\mathbf{x})}{\partial x} & 0 \\ 0 & \dfrac{\partial\varphi_i(\mathbf{x})}{\partial y} \\ \dfrac{\partial\varphi_i(\mathbf{x})}{\partial y} & \dfrac{\partial\varphi_i(\mathbf{x})}{\partial x} \end{bmatrix} \tag{16}$$

2.3. Some properties of FEM

Property 1 (*Lower bound property*). For the elasticity problems with homogeneous essential boundary conditions, the strain energy obtained from the displacement-based fully compatible FEM model

is a lower bound of the exact strain energy. We have provided a brief proof for this property in the previous work and similar discussions on this issue can also be found in the book by Zienkiewicz and Taylor [2].

Property 2 (*Monotonic property*). Assume a sequence of m meshes $M_1, M_2, \ldots, M_m$, in which the nodes in M_i contain the nodes in M_{i-1} $(i = 2, 3, \ldots, m)$, we have the following inequalities:

$$\tilde{U}(\tilde{\boldsymbol{\varepsilon}}_{M_1}) \leqslant \tilde{U}(\tilde{\boldsymbol{\varepsilon}}_{M_2}) \leqslant \cdots \leqslant \tilde{U}(\tilde{\boldsymbol{\varepsilon}}_{M_{n_m}}) \leqslant U_0(\boldsymbol{\varepsilon}_0) \tag{17}$$

where $\tilde{U}(\tilde{\boldsymbol{\varepsilon}}_{M_i})$ is the computed strain energy of FEM solution with the M_i mesh and $U_0(\boldsymbol{\varepsilon}_0)$ is the exact strain energy calculated using the exact strain solution $\boldsymbol{\varepsilon}_0$. This property can be shown easily following the arguments given by Oliveira [11].

Property 3 (*Reproducibility property*). If the exact solution is contained in the space of the FEM shape functions, solution of the compatible FEM model will be exact. Proof of this property can also be found in the paper by Oliveira [11].

3. Briefing on the LC-PIM

3.1. Construction of PIM shape functions

The PIM obtains the approximation by forcing the interpolation function to be satisfied at each scattered node within the local support domain of the point of interest [12]. So far two types of PIM shape functions have been developed with different types of basis functions, i.e., polynomial basis functions [7] and radial basis functions [13]. In the simplest setting of LC-PIM, the polynomial PIM is employed and background cells of three-node triangles are used for the construction of shape functions. In our previous work, both linear and quadratic interpolation procedures are used. The LC-PIM using linear shape functions is very efficient and even more efficient than the conventional FEM using linear triangular elements [6]. In the present work, therefore, the simplest linear interpolation is employed, which means the LC-PIM uses exactly the same interpolation as in the linear FEM.

3.2. Discretized system equations

In the LC-PIM, the generalized Galerkin weak form, which is derived from the Hellinger–Reissner's two-field variational principle, has been proved to be a valid weak form for LC-PIM [8].

$$\int_\Omega \delta(\widehat{\boldsymbol{\varepsilon}}(\mathbf{u}))^{\mathrm{T}} \mathbf{D}(\widehat{\boldsymbol{\varepsilon}}(\mathbf{u}))\,\mathrm{d}\Omega - \int_\Omega \delta\mathbf{u}^{\mathrm{T}}\mathbf{b}\,\mathrm{d}\Omega - \int_{\Gamma_t} \delta\mathbf{u}^{\mathrm{T}}\hat{\mathbf{t}}\,\mathrm{d}\Gamma = 0 \tag{18}$$

where $\widehat{\boldsymbol{\varepsilon}}(\mathbf{u})$ is the assumed strain which is the function of the assumed displacement $\mathbf{u}$. Substituting the linear PIM approximation, which is as same as that in the linear FEM shown Eq. (11), into Eq. (18), a set of discretized system equations can be obtained in the following matrix form:

$$\widehat{\mathbf{K}}\,\widehat{\mathbf{d}} = \widehat{\mathbf{f}} \tag{19}$$

In obtaining Eq. (19), a nodal integration scheme with strain smoothing operation is used to perform the numerical integration over the problem domain Ω.

3.3. Nodal integration with strain smoothing

The node-based integration scheme proposed by Chen et al. [14] is used in the LC-PIM. In such a nodal integration scheme, the problem domain Ω is divided into smoothing domains associated with nodes: $\Omega = \Omega_1 \cup \Omega_2 \cup \cdots \cup \Omega_N$ and $\Omega_i \cap \Omega_j = \emptyset (i \neq j)$, in which N is the number of total field nodes. Based on the background cells of triangles, smoothing domain Ω_k for node k is formed by connecting sequentially the mid-edge-point to the centroids of the surrounding triangles of the node (shown in Fig. 1).

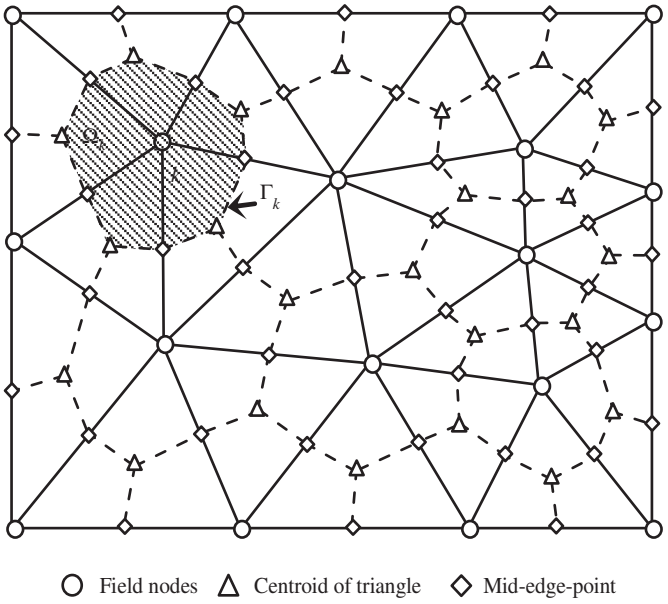

Fig. 1. Illustration of background triangular cells and the smoothing domain for each node (the smoothing domain is created by sequentially connecting the centroids with the mid-edge-points of the surrounding triangles of this node).

Using the nodal integration scheme, the entries of the stiffness matrix $\widehat{\mathbf{K}}$ is represented as

$$\widehat{\mathbf{K}}_{ij} = \sum_{k=1}^{N} \widehat{\mathbf{K}}_{ij(k)} \tag{20}$$

where $\widehat{\mathbf{K}}_{ij(k)}$ is the stiffness matrix of node k which is calculated by

$$\widehat{\mathbf{K}}_{ij(k)} = \int_{\Omega_k} \widehat{\mathbf{B}}_i^{\mathrm{T}} \mathbf{D} \widehat{\mathbf{B}}_j\,\mathrm{d}\Omega = \widehat{\mathbf{B}}_i^{\mathrm{T}} \mathbf{D} \widehat{\mathbf{B}}_j A_k \tag{21}$$

where $\widehat{\mathbf{B}}$ is the smoothed strain matrix and A_k is the area of the smoothing domain of node k.

The entries of the force vector $\widehat{\mathbf{f}}$ in Eq. (19) is expressed as

$$\widehat{\mathbf{f}}_i = \sum_{k \in N_{\mathrm{infl}}} \widehat{\mathbf{f}}_{i(k)} \tag{22}$$

where N_{infl} is the number of nodes in the influence domain of node k (including node k). As linear PIM shape functions are used, it is exactly the number of nodes that is directly connected to node k. $\widehat{\mathbf{f}}_{i(k)}$ can be further calculated as

$$\widehat{\mathbf{f}}_{i(k)} = \int_{\Gamma_{t(k)}} \boldsymbol{\Phi}_i \hat{\mathbf{t}}\,\mathrm{d}\Gamma + \int_{\Omega_{(k)}} \boldsymbol{\Phi}_i \mathbf{b}\,\mathrm{d}\Omega \tag{23}$$

In the LC-PIM, the smoothed strain in Eq. (18) is obtained using the node-based strain smoothing operation as follows [14]:

$$\widehat{\boldsymbol{\varepsilon}}_k = \int_{\Omega_k} \boldsymbol{\varepsilon}(\mathbf{x}) \widehat{\mathbf{W}}(\mathbf{x} - \mathbf{x}_k)\,\mathrm{d}\Omega \tag{24}$$

where $\widehat{\boldsymbol{\varepsilon}}_k$ is the smoothed strain for node k, $\widehat{\mathbf{W}} = \lfloor \widehat{W} \;\; \widehat{W} \;\; \widehat{W} \rfloor$ is a diagonal matrix of smoothing function $\widehat{W}$. Using the following

constant smoothing function

$$\widehat{W}(\mathbf{x}-\mathbf{x}_k)=\begin{cases}1/A_k & \mathbf{x}\in\Omega_k\\ 0 & \mathbf{x}\notin\Omega_k\end{cases} \tag{25}$$

and applying divergence theorem, we can obtain the smoothed strain which is constant over the smoothing domain Ω_k as follows:

$$\widehat{\boldsymbol{\varepsilon}}_k=\frac{1}{A_k}\int_{\Omega_k}\boldsymbol{\varepsilon}(\mathbf{x})\,\mathrm{d}\Omega=\frac{1}{A_k}\int_{\Gamma_k}\mathbf{L}_n\mathbf{u}(\mathbf{x})\,\mathrm{d}\Gamma=\widehat{\boldsymbol{\varepsilon}}_k(\mathbf{u}) \tag{26}$$

where Γ_k is the boundary of the smoothing domain Ω_k. Substituting the PIM approximation function into Eq. (26), the smoothed strain can be expressed in the following matrix form:

$$\widehat{\boldsymbol{\varepsilon}}_k=\sum_{i\in N_{\mathrm{infl}}}\widehat{\mathbf{B}}_i(\mathbf{x}_k)\mathbf{U}_i \tag{27}$$

where $\widehat{\mathbf{B}}_i(\mathbf{x}_k)$ is the smoothed strain matrix expressed as

$$\widehat{\mathbf{B}}_i(\mathbf{x}_k)=\begin{bmatrix}\widehat{b}_{ix}(\mathbf{x}_k) & 0\\ 0 & \widehat{b}_{iy}(\mathbf{x}_k)\\ \widehat{b}_{iy}(\mathbf{x}_k) & \widehat{b}_{ix}(\mathbf{x}_k)\end{bmatrix} \tag{28}$$

in which the elements of the smoothed strain matrix can be calculated numerically using Gauss integration along boundary Γ_k as follows:

$$\widehat{b}_{il}=\frac{1}{A_k}\sum_{m=1}^{N_s}\left[\sum_{n=1}^{N_g}w_n\varphi_i(\mathbf{x}_{mn})n_l(\mathbf{x}_m)\right]\quad(l=x,y) \tag{29}$$

where N_s is the number of segments of the boundary Γ_k, N_g is the number of Gauss points used in each segment, w_n is the corresponding weight number of Gauss integration scheme, and n_l is the unit outward normal corresponding to each segment on the smoothing domain boundary. As linear PIM interpolation is employed, $N_g=1$ is used in the present work.

3.4. Properties of the LC-PIM

Instead of using the compatible strain that is obtained from the compatibility equation, LC-PIM uses smoothed strain (obtained from Eq. (27)) over smoothing cells of the field nodes. The strain smoothing operation can soften the structure and improves the accuracy of the method [8]. As constant smoothing function is used in the present work, the smoothed strains are constant within the smoothing cells. Then the LC-PIM solutions satisfy the equilibrium equations (free of body force) at any point in the entire problem domain, except on the interfaces of the smoothing cells. The displacement field of the LC-PIM is compatible in the global problem domain. For the elasticity problem with homogeneous essential boundary conditions, LC-PIM possesses the following intrinsic properties.

Property 1 (*the LC-PIM is variationally consistent*). Using the smoothed strain to replace the compatible strain, the LC-PIM has been proved satisfies the following orthogonal condition:

$$\int_\Omega\widehat{\boldsymbol{\varepsilon}}^{\mathrm{T}}\mathbf{D}\boldsymbol{\varepsilon}\,\mathrm{d}\Omega=\int_\Omega\widehat{\boldsymbol{\varepsilon}}^{\mathrm{T}}\mathbf{D}\,\widehat{\boldsymbol{\varepsilon}}\,\mathrm{d}\Omega \tag{30}$$

which implies that LC-RPIM is variationally consistent [15]. Detailed examination of the above statement can be found in the previous work [8].

Property 2 (*the LC-PIM possesses the upper bound property*). For the elasticity problem with homogeneous essential boundary conditions, the LC-RPIM solution (in energy norm) is always no less than that of displacement-based fully compatible FEM and is no less than that of exact solution except a few trivial cases; for example, only one element is used to represent the entire problem domain.

This property has been proved theoretically and demonstrated using intensive numerical studies in the previous work. Therefore, we omit the proof here and refer the reader to the recent paper by Liu and Zhang [8].

4. Adaptive procedure

Error indicator and refinement strategy are two important issues for an adaptive procedure. In the present work, a residual-based error indicator and a simple *h*-type refinement scheme are employed to perform the adaptive analyses using LC-PIM and FEM.

4.1. Residual-based error indicator

In the present work, a residual-based error indicator is defined as follows for each background cell:

$$\eta_i=\|\mathbf{L}_d^{\mathrm{T}}\boldsymbol{\sigma}^*\|_{L_2} \tag{31}$$

where η_i is the residual error of background cell i, which is calculated based on the elemental stresses $\boldsymbol{\sigma}^*$. With the background cells of three-node triangles, the elemental stress can be approximates as

$$\boldsymbol{\sigma}^*=\sum_{j=1}^{3}\boldsymbol{\Phi}_j\boldsymbol{\sigma}_j \tag{32}$$

where $\boldsymbol{\Phi}$ is vector of shape functions and σ represents the nodal stress vector. Then Eq. (31) can be further written as

$$\begin{aligned}\eta_i&=S_i\sqrt{\left(\frac{\partial\sigma_{xx}^*}{\partial x}+\frac{\partial\tau_{xy}^*}{\partial y}\right)^2+\left(\frac{\partial\sigma_{yy}^*}{\partial y}+\frac{\partial\tau_{xy}^*}{\partial x}\right)^2}\\ &=S_i\sqrt{\left(\sum_{j=1}^{3}\frac{\partial\phi_j}{\partial x}\sigma_{xx}^j+\sum_{i=1}^{3}\frac{\partial\phi_j}{\partial y}\tau_{xy}^j\right)^2+\left(\sum_{j=1}^{3}\frac{\partial\phi_j}{\partial y}\sigma_{yy}^j+\sum_{i=1}^{3}\frac{\partial\phi_j}{\partial x}\tau_{xy}^j\right)^2}\\ &=S_i\sqrt{\left(\sum_{j=1}^{3}\left(\frac{\partial\phi_j}{\partial x}\sigma_{xx}^j+\frac{\partial\phi_j}{\partial y}\tau_{xy}^j\right)\right)^2+\left(\sum_{j=1}^{3}\left(\frac{\partial\phi_j}{\partial y}\sigma_{yy}^j+\frac{\partial\phi_j}{\partial x}\tau_{xy}^j\right)\right)^2}\end{aligned} \tag{33}$$

where S_i is the area of background cell i.

Note that for the LC-PIM, the nodal stresses used in Eqs. (32) and (33) can be obtained directly based on the displacement results. For the linear FEM, we first use Zienkiewicz–Zhu recovery technique [2] to compute the nodal stresses and then substitute the results into Eq. (33).

The error indicator is used only to give an indication on where in the problem domain has large error, so that a refinement can be carried out there. The exact error is the solution of the problem to be determined by the LC-PIM (upper bound) and FEM (lower bound).

4.2. Local refinement criteria

Using Eq. (33), the residual error for each background cell can be calculated. The refinement on a cell is performed when the following local criteria is met.

$$\eta_i\geqslant\eta_l \tag{34}$$

where η_i is the residual error of cell i and η_l is the local critical value of residual error in a particular adaptive step which is defined as follows:

$$\eta_l=\kappa_l\eta_{\max} \tag{35}$$

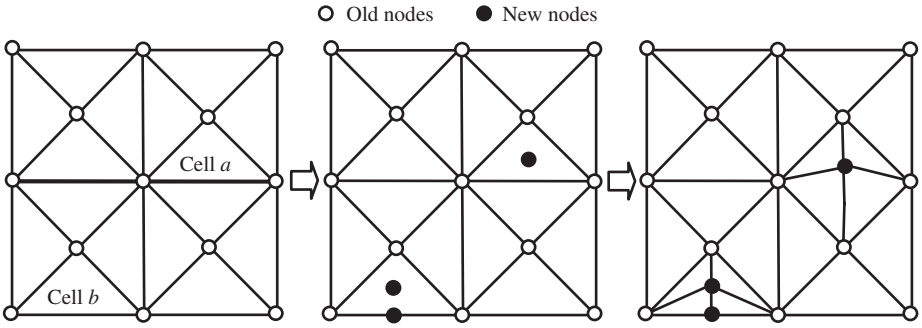

Fig. 2. Illustration of the *h*-type refinement strategy.

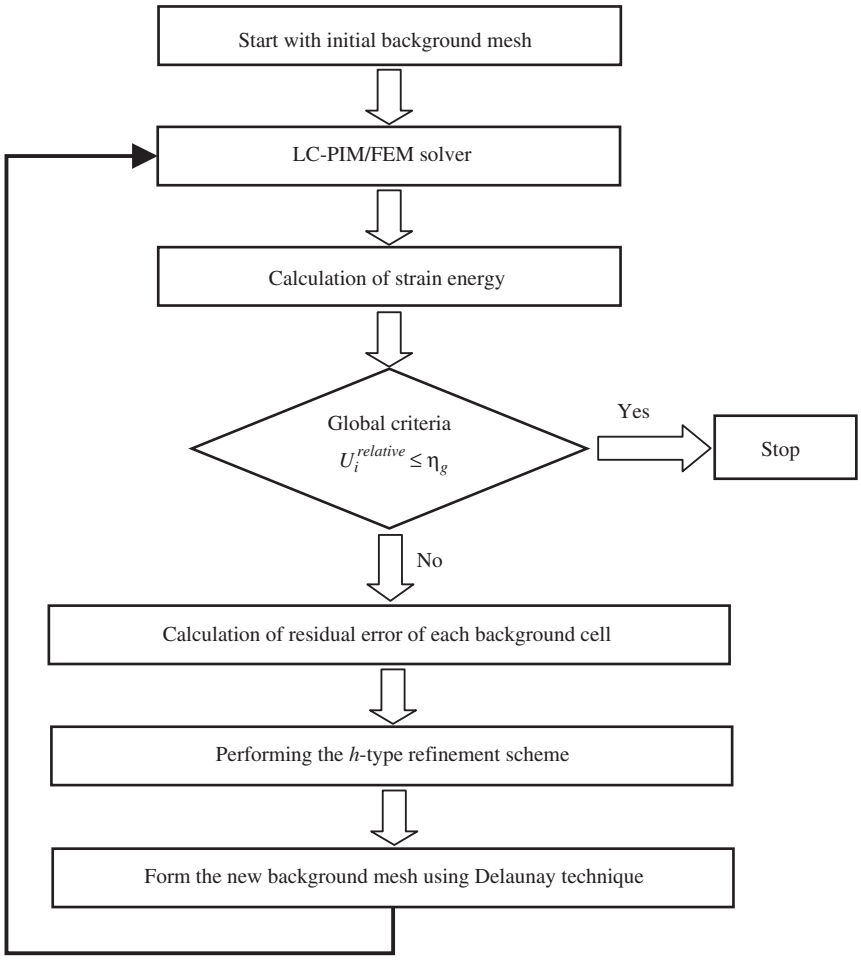

Fig. 3. Flow chart of the adaptive procedure.

where κ_1 is a constant number which will be predefined before the adaptive procedure and $\eta_{\max}$ is the maximum value of residual errors throughout all the background cells at this adaptive step.

4.3. Global stopping criteria

With the increase of DOFs in the model, the computed strain energies of LC-PIM and FEM will converge, respectively, from above and below, to the exact solution. Making use of this property, we use the following global criteria to decide when to terminate the adaptive analysis:

$$U_i^{\text{relative}} \leqslant \eta_g \quad (i \geqslant 2) \tag{36}$$

where η_g is a predefined threshold of strain energy error and U_i^{relative} is the relative error of strain energy in the adaptive process of step i which is defined as follows:

$$U_i^{\text{relative}} = \left| \frac{U_i - U_{i-1}}{U_{i-1}} \right| \times 100\% \tag{37}$$

where U_i and U_{i-1} are values of computed strain energy at step i and step $i-1$ of the adaptive analysis, respectively.

By changing the value of η_g, we can control the adaptive analysis and obtain solutions with desired strain energy bounds: a bigger value of η_g leads to fewer steps of adaptive analysis and looser bounds to exact strain energy; a smaller value of η_g leads to more adaptive steps and tighter bounds to exact strain energy.

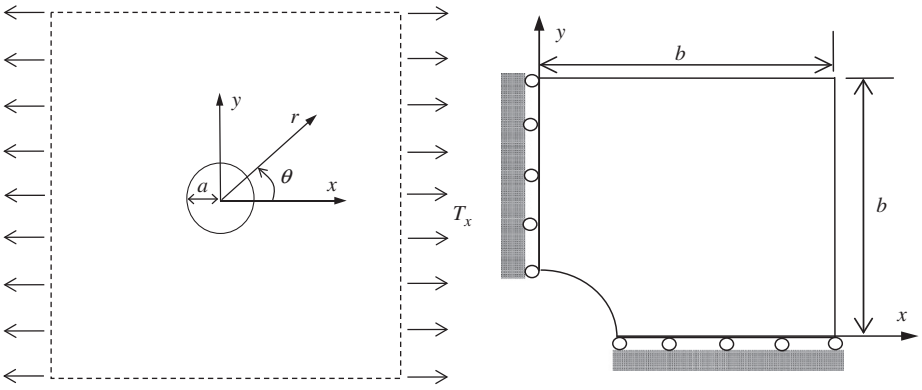

Fig. 4. Infinite solid with a circular hole subjected to uniform tensile and its quadrant model.

4.4. Adaptive scheme

In this work, a simple yet effective refinement scheme based on Delaunay triangular cells is employed. In each adaptive step, refinement will be performed by simply adding nodes in the cell which meets the local refinement criteria. Initially, triangular cells are created and the cells are classified into two groups: interior cells and edge cells. An interior cell is a cell that has no edge on the boundaries of the problem domain, and an edge cell is a cell which has at least one edge on the boundaries. As shown in Fig. 2, cell *a* and cell *b* are interior and edge cells, respectively. If an interior cell needs to be refined, one new node will be added at the centroid of this triangle; for an edge cell, two new nodes will be added at the centroid and the midpoint of the boundary edge, respectively (see Fig. 2). Finally, the formation of the new background mesh is created by using the Delaunay technique based on the new nodes configuration. This simple *h*-type refinement scheme can be easily implemented and possesses the following advantages: the triangular cells can be generated efficiently and automatically without manual operation for domains of arbitrary shapes and the information at the nodes of old mesh is preserved.

The flow chart of the adaptive procedure is illustrated in Fig. 3 which is used to guide the adaptive analyses for both LC-PIM and FEM.

5. Numerical examples

A number of numerical examples are studied in this section. Materials of the problems are linear elastic and units used are based on international standard unit system unless specially mentioned.

5.1. Infinite solid with a circular hole

A benchmark problem is studied first, which is an infinite two-dimensional solid with a central circular hole of radius a and subjected to a unidirectional tensile T_x. Owing to the two-fold symmetry, only the upper right quadrant of the problem modeled and investigated (with the dimensions of b in x and y directions as shown in Fig. 4). Symmetry conditions are imposed on the left and the bottom edges. The analytical solution of stress components [16] is

$$\sigma_{xx} = T_x\left\{1 - \frac{a^2}{r^2}\left[\frac{3}{2}\cos(2\theta) + \cos(4\theta)\right] + \frac{3a^4}{2r^4}\cos(4\theta)\right\} \tag{38}$$

$$\sigma_{yy} = -T_x\left\{\frac{a^2}{r^2}\left[\frac{1}{2}\cos(2\theta) - \cos(4\theta)\right] + \frac{3a^4}{2r^4}\cos(4\theta)\right\} \tag{39}$$

$$\sigma_{xy} = -T_x\left\{\frac{a^2}{r^2}\left[\frac{1}{2}\sin(2\theta) + \sin(4\theta)\right] - \frac{3a^4}{2r^4}\sin(4\theta)\right\} \tag{40}$$

Table 1
Strain energy bounds for the infinite solid with circular hole problem

Mesh	1	2	3	4	5	6
LC-PIM (uniform)						
DOF	126	270	554	1154	2660	5700
$U_i(\times 10^{-4})$	0.436776	0.435158	0.433938	0.433280	0.432856	0.432679
FEM (uniform)						
DOF	126	270	554	1154	2660	5700
$U_i(\times 10^{-4})$	0.422749	0.428787	0.430231	0.431238	0.431962	0.432249
LC-PIM (adaptive)						
DOF	126	202	296	502	1332	–
$U_i(\times 10^{-4})$	0.436776	0.434907	0.433569	0.432829	0.432571	–
FEM (adaptive)						
DOF	126	176	262	522	1248	2982
$U_i(\times 10^{-4})$	0.422749	0.428488	0.430752	0.431718	0.432201	0.432397

Note: U_i is the computed value of strain energy of the problem at step i of mesh situations.

where (r,θ) are the polar coordinates and θ is measured counterclockwise from the positive x-axis. The inner boundary of the hole is traction free and the right and the upper edges are imposed with the tractions based on the analytical solutions in the above equations. The displacement components corresponding to the stresses are expressed as

$$u_r = \frac{T_x}{4\mu}\left\{r\left[\frac{(\kappa-1)}{2} + \cos(2\theta)\right] + \frac{a^2}{r}\left[1+(1+\kappa)\cos(2\theta)\right] - \frac{a^4}{r^3}\cos(2\theta)\right\} \tag{41}$$

$$u_\theta = \frac{T_x}{4\mu}\left[(1-\kappa)\frac{a^2}{r} - r - \frac{a^4}{r^3}\right]\sin(2\theta) \tag{42}$$

where

$$\mu = \frac{E}{2(1+\nu)}$$
$$\kappa = \begin{cases} 3-4\nu & \text{plane strain} \\ \dfrac{3-\nu}{1+\nu} & \text{plane stress} \end{cases} \tag{43}$$

Plane stress is considered and the parameters are taken as $E = 3.0 \times 10^7$, $\nu = 0.3$, $a = 1$, $b = 5$ and $T_x = 10$.

For this problem, a reference value of the exact strain energy is calculated using the stress components provided in Eqs. (38)–(40), which is 0.432533×10^{-4}. To perform the adaptive analysis, the controlling parameters $\kappa_l = 0.08$ and $\eta_g = 0.5\%$ are used for the local and global criteria, respectively. Starting with the initial mesh of 63 uniformly distributed nods, five and six adaptive steps are

implemented, respectively, for LC-PIM and FEM to meet the global criteria. For comparison, six models of uniformly distributed nodes are also computed using FEM and LC-PIM. The results obtained for the strain energy bounds are summarized in Table 1, and plotted in Fig. 5.

It can be clearly found that the strain energy of the FEM model is always smaller than the reference one and converge to it with the increase of DOFs. On the contrary, the strain energy of the LC-PIM model is always larger than the reference one and will converge to it with the increase of DOFs. These results demonstrate that FEM and LC-PIM provide lower and upper bounds of the exact strain energy, respectively. Compared with the results of uniform models, the strain energy values of the adaptive models converge much faster to the reference one and a much tighter bound to the exact strain energy is obtained at the final adaptive analysis step. It means that we can effectively obtain a narrow bound of the exact strain energy of elasticity problem by using FEM together with LC-PIM with adaptive analyses.

Based on the analytical solution provided in Eqs. (35)–(39), errors in displacement and energy norm are calculated according to the following definitions.

$$e_d = \sqrt{\frac{\sum_{i=1}^{n}(u_i^{\text{exact}} - u_i^{\text{numerical}})^2}{\sum_{i=1}^{n}(u_i^{\text{exact}})^2}} \tag{44}$$

$$e_e = \frac{1}{A}\sqrt{\frac{1}{2}\int_{\Omega}(\boldsymbol{\varepsilon}^{\text{exact}} - \boldsymbol{\varepsilon}^{\text{numerical}})^{\mathrm{T}}\mathbf{D}(\boldsymbol{\varepsilon}^{\text{exact}} - \boldsymbol{\varepsilon}^{\text{numerical}})\,\mathrm{d}\Omega} \tag{45}$$

Fig. 6 shows the convergence status for FEM and LC-PIM. It can be observed that both FEM and LC-PIM obtain much higher convergence rate when the adaptive procedure is employed. This also demonstrates the effectiveness of the present adaptive analysis procedure. Fig. 7 shows the nodes distributions at each adaptive step for the LC-PIM. It can be found that the refinement is activated exactly in the regions with a significant stress concentration, which demonstrates that the proposed error indicator is able to identify the singularity points accurately.

5.2. L-shaped plate

An L-shaped plate subjected to uniform tensile force in the horizontal direction is studied (shown in Fig. 8). The plate is constrained in x and y direction along the right and upper edges, respectively. Plane stress problem is considered with the parameters $E=3.0\times10^7$, $v=0.3$, $a=5$ and $p=10$.

For the adaptive analyses using LC-PIM and FEM, controlling parameters $\kappa_l=0.08$ and $\eta_g=0.3\%$ are used and six adaptive steps are performed for both these two methods. Four uniform refinement models are also studied and the computed strain energy bounds are listed in Table 2, and plotted in Fig. 9, together with the results obtained using the adaptive models. As the exact strain energy for this problem is not available, a reference value of 0.518963×10^{-3} is obtained by using FEM with very fine mesh (total 13 654 nodes). The results show that LC-PIM and FEM provide upper and lower bound solutions to the exact strain energy, respectively. Performing the adaptive technique, the computed strain energy values converge much faster and a much tighter bound to the strain energy can be obtained compared with the results of uniform refinement models.

The nodes distributions at each adaptive step for the LC-PIM are plotted in Fig. 10. It can be found that the occurrence of refinement properly concentrates around the origin, where situation of singularity exists.

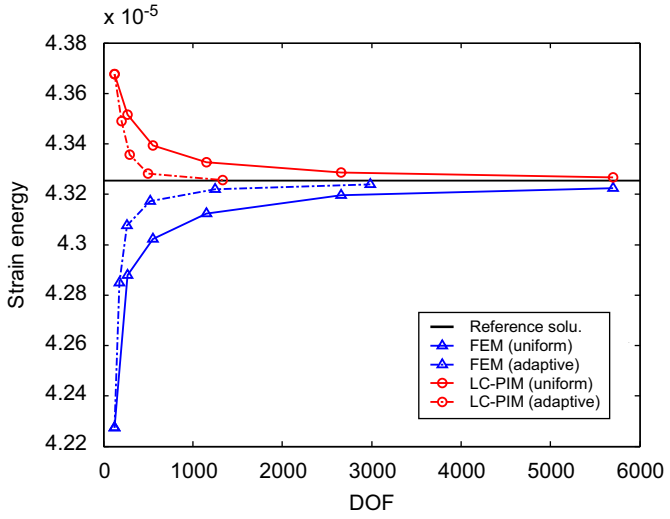

Fig. 5. Strain energy bound for the problem of infinite solid with circular hole: the upper and bound solutions are obtained using LC-PIM and FEM, respectively.

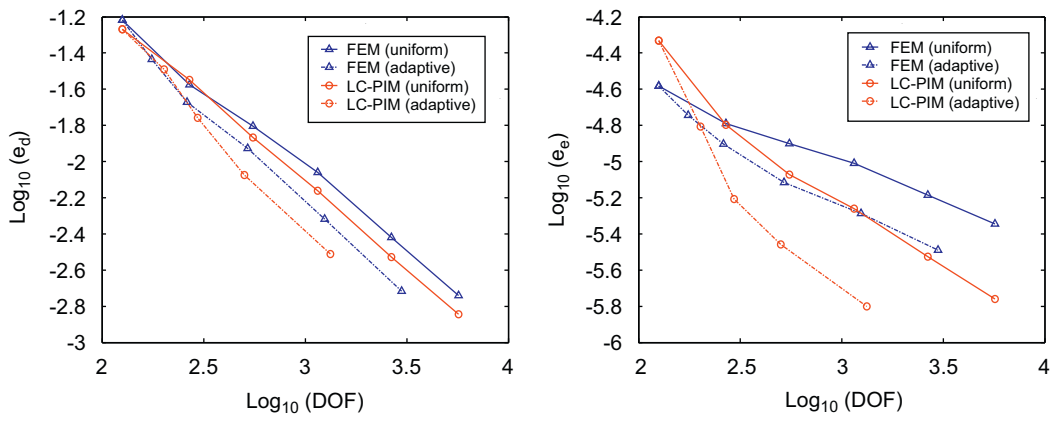

Fig. 6. Comparison of convergence via the problem of infinite solid with circular hole.

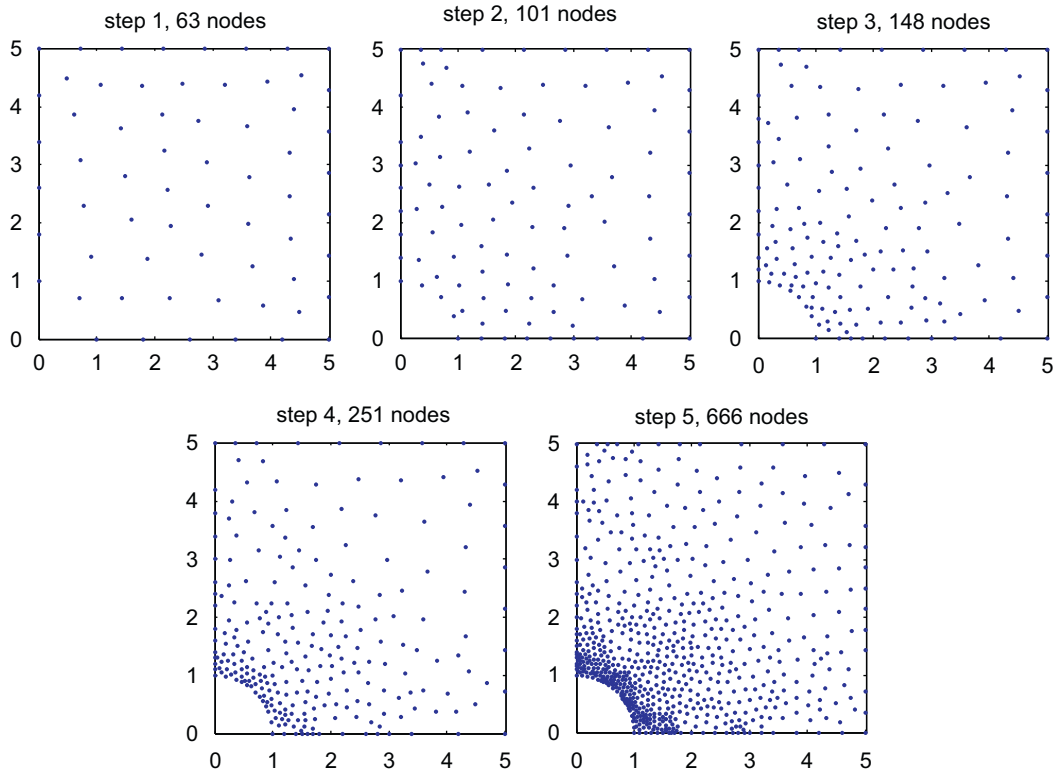

Fig. 7. Nodes distributions of adaptive analysis using LC-PIM for the problem of infinite solid with circular hole.

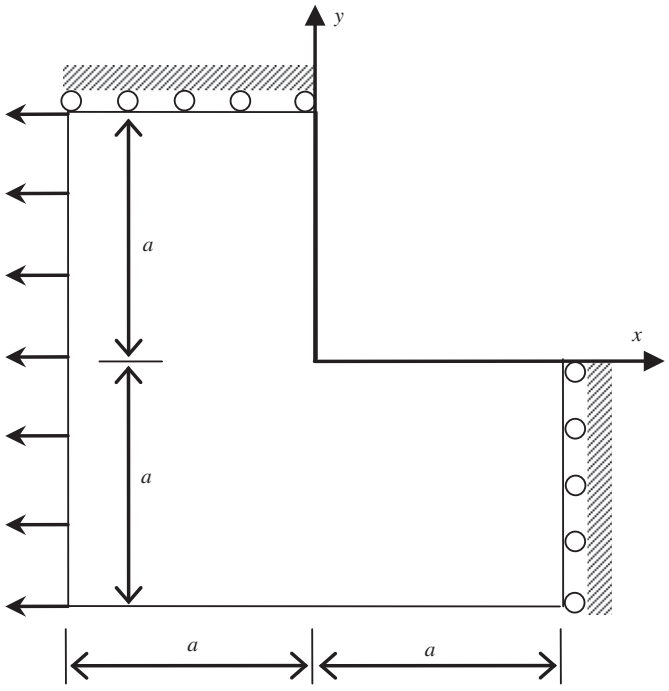

Fig. 8. L-shaped plate subjected to uniform tensile.

5.3. Short cantilever solid

A short cantilever solid problem is studied, which is a square solid fixed on the left edge and subjected to uniform pressure on the upper edge (shown in Fig. 11). Considered as plane strain problem, a reference value (0.951848) of the exact strain energy for this problem is provided in the works of Steeb et al. [17] with the parameters of $E = 1.0$, $\nu = 0.3$ and $P = 1.0$.

Table 2
Strain energy bounds for the L-shaped plate

Mesh	1	2	3	4	5	6
LC-PIM (uniform)						
DOF	218	738	2860	4388	–	–
$U_i(\times 10^{-3})$	0.548144	0.530171	0.522987	0.521896	–	–
FEM (uniform)						
DOF	218	738	2860	4388	–	–
$U_i(\times 10^{-3})$	0.495727	0.510419	0.515879	0.516686	–	–
LC-PIM (adaptive)						
DOF	218	488	968	1528	2468	3860
$U_i(\times 10^{-3})$	0.548144	0.533227	0.525512	0.523548	0.521708	0.520987
FEM (adaptive)						
DOF	218	406	692	1524	2406	4322
$U_i(\times 10^{-3})$	0.495727	0.504576	0.509877	0.514141	0.516300	0.517442

Adaptive analyses are implemented with the controlling parameters $\kappa_1 = 0.08$ and $\eta_g = 0.5\%$ and four and six adaptive steps are performed for LC-PIM and FEM, respectively. Four uniform refinement models are also computed. The calculated values of strain energy are listed in Table 3, and plotted in Fig. 12. The results show that LC-PIM and FEM provide upper and lower bounds to the exact strain energy, respectively. By using the present adaptive procedure, the calculated strain energy converges much faster and a much tighter bound to the exact strain energy can be obtained efficiently.

5.4. Mode-I crack problem

A square plate containing a crack and subjected to boundary conditions prescribed by the near crack tip field solution is studied,

which is shown in Fig. 13. The plate has a side of $2a$ and the length of the crack is a. This is so-called Griffith mode-I crack problem with the following analytical solutions [18]:

$$\sigma_{xx} = \frac{K_I}{\sqrt{2\pi r}} \cos\frac{\theta}{2}\left(1 - \sin\frac{\theta}{2}\sin\frac{3\theta}{2}\right) \quad (46)$$

$$\sigma_{yy} = \frac{K_I}{\sqrt{2\pi r}} \cos\frac{\theta}{2}\left(1 + \sin\frac{\theta}{2}\sin\frac{3\theta}{2}\right) \quad (47)$$

$$\sigma_{xy} = \frac{K_I}{\sqrt{2\pi r}} \sin\frac{\theta}{2}\cos\frac{\theta}{2}\cos\frac{3\theta}{2} \quad (48)$$

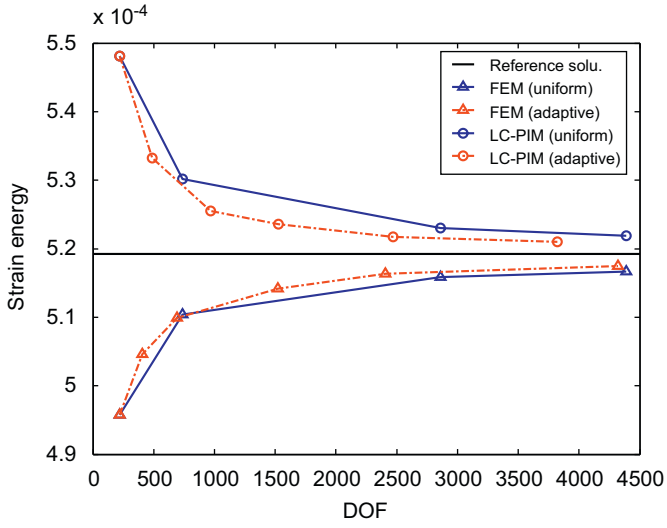

Fig. 9. Strain energy bound for the problem of L-shaped plate: the upper and bound solutions are obtained using LC-PIM and FEM, respectively.

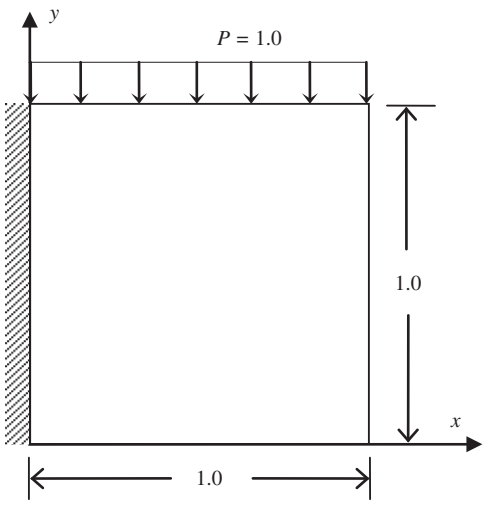

Fig. 11. Short cantilever solid.

Table 3
Strain energy bounds for the short cantilever solid

Mesh	1	2	3	4	5	6
LC-PIM (uniform)						
DOF	82	290	1090	2402	–	–
U_i	1.002011	0.981604	0.959149	0.955899	–	–
FEM (uniform)						
DOF	82	290	1090	2402	–	–
U_i	0.874266	0.921759	0.940585	0.945535	–	–
LC-PIM (adaptive)						
DOF	82	232	372	792	–	–
U_i	1.002011	0.982259	0.962103	0.958651	–	–
FEM (adaptive)						
DOF	82	224	432	738	1062	2098
U_i	0.874266	0.914675	0.934042	0.940479	0.945640	0.948167

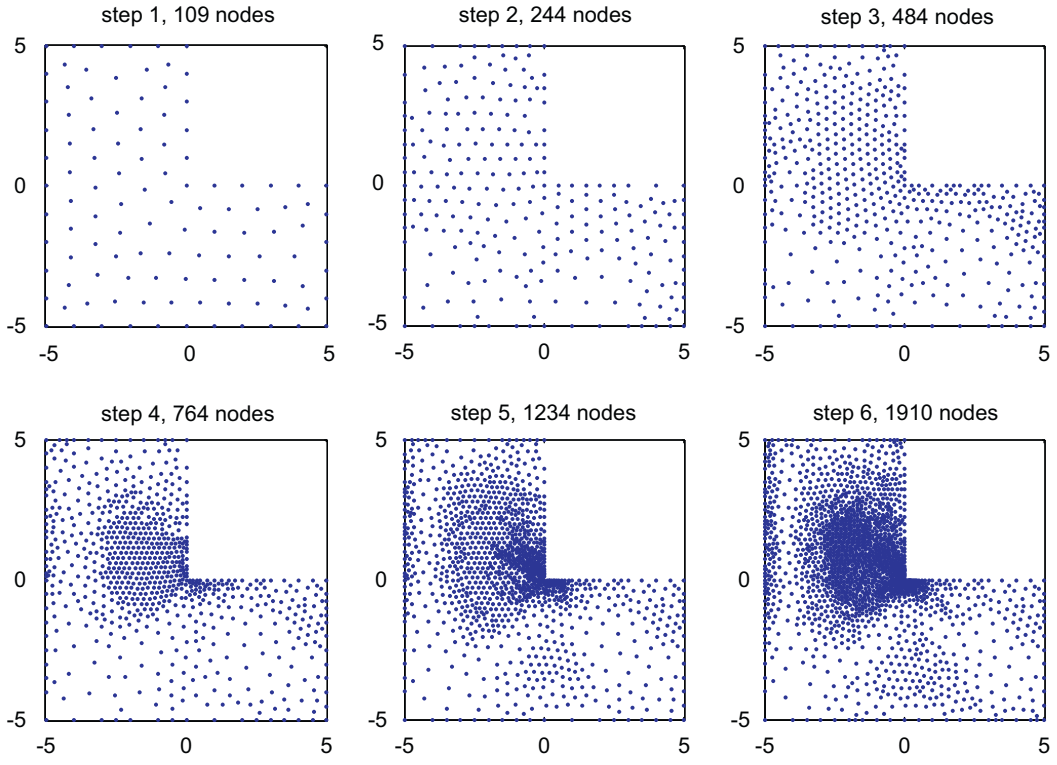

Fig. 10. Nodes distributions of adaptive analysis using LC-PIM for the problem of L-shaped plate.

where K_I is the stress intensity factor which is assumed to be $K_I=\sqrt{2\pi}$ in this case. Owning to the symmetry about x-axis, the upper half of the plate is modeled for study (see Fig. 13). To extend the analytical solution to the whole domain, the exact traction calculated based on Eqs. (46)–(48) are applied on the upper, the right and the left edges of the model. The symmetric conditions are applied on the bottom edge as shown in Fig. 13. The problem is studied as plain strain with the parameters of $E=3.0\times10^7, \nu=0.3$ and $a=1$.

To perform the adaptive analyses using LC-PIM and FEM, the controlling parameters $\kappa_l=0.08$ and $\eta_g=0.5\%$ are used and five and six adaptive steps are implemented for LC-PIM and FEM, respectively. The strain energy bound obtained using both the adaptive models and four uniform refinement models are summarized in Table 4, and plotted in Fig. 14. A reference value of the exact strain energy is obtained based on the analytical solutions provided in Eqs. (46)–(48), which is 0.495039×10^{-7} for the present problem. It can be found that by using LC-PIM together with FEM with adaptive analysis procedure, a much tighter bound to the exact energy can be obtained efficiently. Fig. 15 shows the convergence study in terms of displacement and energy errors. The picture indicates that much higher convergence rates can be achieved for both LC-PIM and FEM by using the adaptive models, which also demonstrates the effectiveness of the present adaptive procedure.

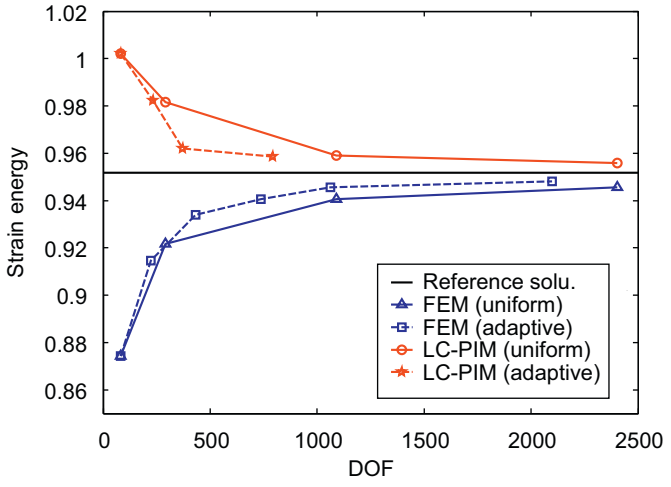

Fig. 12. Strain energy bound for the problem of short cantilever solid: the upper and bound solutions are obtained using LC-PIM and FEM, respectively.

Table 4
Strain energy bounds for the Model-I crack problem

Mesh	1	2	3	4	5	6
LC-PIM (uniform)						
DOF	90	306	1122	2652	–	–
$U_i(\times10^{-7})$	0.540634	0.523885	0.511233	0.506144	–	–
FEM (uniform)						
DOF	90	306	1122	2652	–	–
$U_i(\times10^{-7})$	0.428673	0.456935	0.475029	0.482339	–	–
LC-PIM (adaptive)						
DOF	90	246	372	502	868	–
$U_i(\times10^{-7})$	0.540634	0.520274	0.510904	0.500426	0.498550	–
FEM (adaptive)						
DOF	90	186	414	710	1102	1468
$U_i(\times10^{-7})$	0.428673	0.454863	0.478507	0.484937	0.490058	0.492295

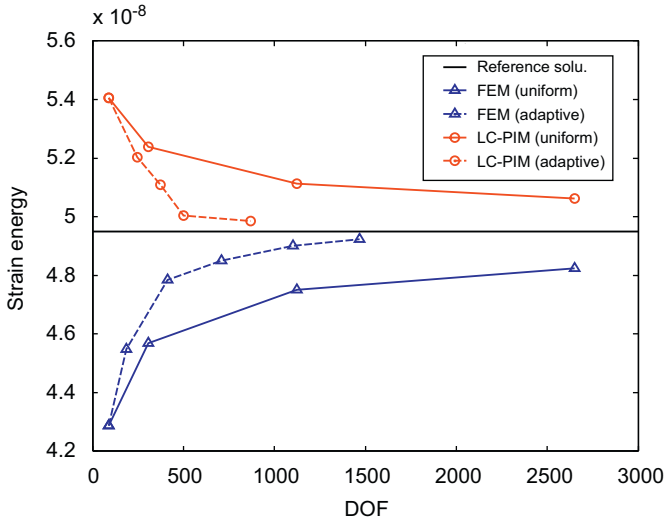

Fig. 14. Strain energy bound for the Mode-I crack problem: the upper and bound solutions are obtained using LC-PIM and FEM, respectively.

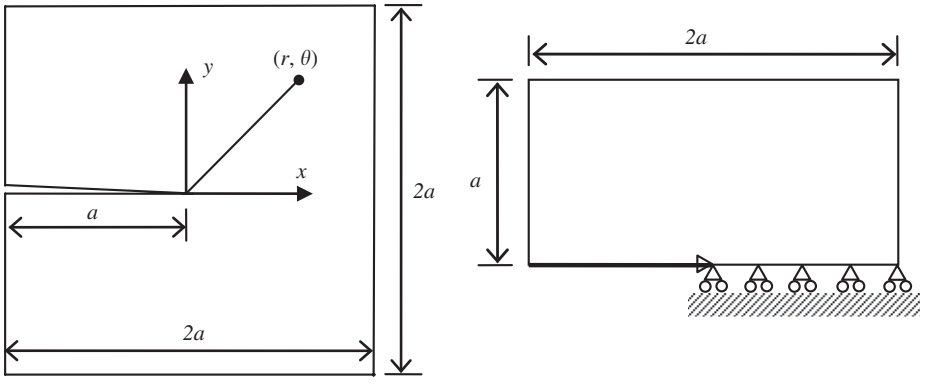

Fig. 13. Mode-I crack problem and its half model.

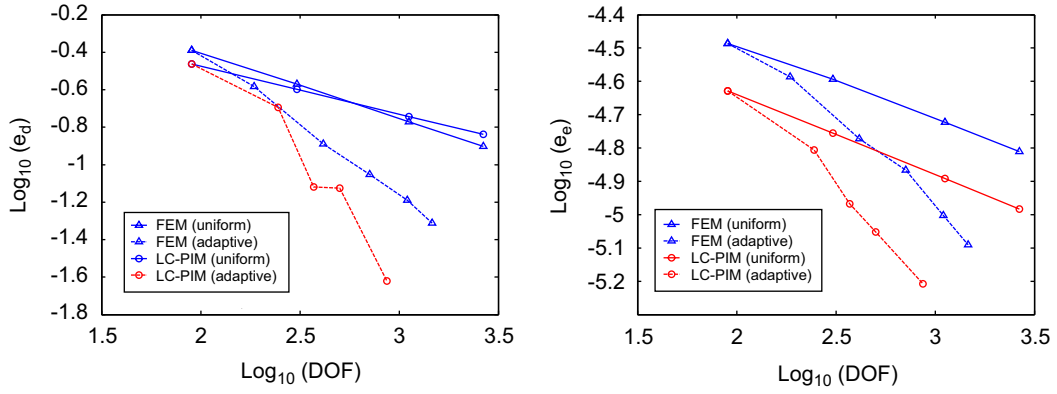

Fig. 15. Comparison of convergence via the Mode-I crack problem.

6. Conclusion

In this work, an efficient adaptive analysis procedure has been developed to obtain certified solution with both upper and lower bounds to the exact strain energy for elasticity problems. Some conclusions can be drawn as follows:

- The proposed adaptive analysis procedure is very simple and can be easily implemented.
- The residual-based error indicator used in the present work can accurately catch the appearance of the steep gradient of stress, and it is sufficiently good enough for identifying areas to be refined.
- The adaptive analysis procedure is performed based on three-node triangular elements which can always be generated efficiently and automatically without manual operation.
- The simple *h*-type refinement scheme is performed by adding new nodes in the old mesh and the information of the old nodes can be preserved.
- Compared with the results of uniform models, solutions of the adaptive models converge much faster and tighter bounds to the exact strain energy can be obtained efficiently.
- The proposed procedure is very robust and applicable to generable elasticity problems even for problems with singularity.

We finally claim that using the present procedure, the certified bound of the exact strain energy for the elasticity problems can always be obtained efficiently at any stage in the adaptive process whenever required.

References

[1] G.R. Liu, Meshfree Methods: Moving Beyond the Finite Element Method, CRC Press, Boca Raton, 2002.
[2] O.C. Zienkiewicz, R.L. Taylor, The Finite Element Method, fifth ed., Butterworth Heinemann, Oxford, UK, 2000.
[3] G.R. Liu, S.S. Quek, The Finite Element Method: A Practical Course, Butterworth Heinemann, Oxford, 2003.
[4] B. Fraeijs de Veubeke, Displacement and equilibrium models in the finite element method, in: O.C. Zienkiewicz, G. Hollister (Eds.), Stress analysis, Wiley, London, 2001, pp. 145–197, Reprinted in: Int. J. Numer. Methods Eng. 52 (2001) 284–342.
[5] J.F. Debongnie, H.G. Zhong, P. Beckers, Dual analysis with general boundary conditions, Comput. Meth. Appl. Mech. Eng. 122 (1995) 183–192.
[6] G.R. Liu, G.Y. Zhang, K.Y. Dai, Y.Y. Wang, Z.H. Zhong, G.Y. Li, X. Han, A linearly conforming point interpolation method (LC-PIM) for 2D solid mechanics problems, Int. J. Comput. Methods 2 (4) (2005) 645–665.
[7] G.R. Liu, Y.T. Gu, A point interpolation method for two-dimensional solids, Int. J. Numer. Methods Eng. 50 (2001) 937–951.
[8] G.R. Liu, G.Y. Zhang, Upper bound solution to elasticity problems: a unique property of the linearly conforming point interpolation method (LC-PIM), Int. J. Numer. Methods Eng. 74 (2008) 1128–1161.
[9] G.R. Liu, Y. Li, K.Y. Dai, M.Y. Luan, W. Xue, A linearly conforming RPIM for 2D solid mechanics, Int. J. Comput. Methods 3 (4) (2006) 401–428.
[10] G.R. Liu, X. Xu, G.Y. Zhang, T.T. Nguyen, A superconvergent point interpolation method (SC-PIM) with piecewise linear strain field using triangular mesh, Int. J. Numer. Methods Eng. (2008) (accepted).
[11] R. Oliveira Eduardo, E. De Arantes, Theoretical foundations of the finite element method, Int. J. Solids Struct. 4 (1968) 929–952.
[12] G.R. Liu, Y.T. Gu, An Introduction to Meshfree Methods and Their Programming, Springer, Dordrecht, The Netherlands, 2005.
[13] J.G. Wang, G.R. Liu, A point interpolation meshless method based on radial basis functions, Int. J. Numer. Methods Eng. 54 (2002) 1623–1648.
[14] J.S. Chen, C.T. Wu, S. Yoon, Y. You, A stabilized conforming nodal integration for Galerkin mesh-free methods, Int. J. Numer. Methods Eng. 50 (2001) 435–466.
[15] J.C. Simo, T.J.R. Hughes, Computational Inelasticity, Springer, New York, 1998.
[16] S.P. Timoshenko, J.N. Goodier, Theory of Elasticity, third ed., McGraw-Hill, New York, 1970.
[17] H. Steeb, A. Maute, E. Ramm, Goal-oriented error estimation in solid mechanics, in: Error-Controlled Adaptive Finite Elements in Solid Mechanics, Wiley, West Sussex, UK, 2002.
[18] N. Perrone, H. Liebowitz, D. Mulville, W. Plikey, Fracture Mechanics, University Press of Virginia, Charlottesville, 1978.